Journal of Neuroscience Methods 354 (2021) 109105

Contents lists available at ScienceDirect

Journal of Neuroscience Methods

journal homepage: www.elsevier.com/locate/jneumeth

Selective targeting of striatal parvalbumin-expressing interneurons for transgene delivery

Marcelo Duarte Azevedo [1], Sibilla Sander [1], Cheryl Jeanneret, Soophie Olfat [2], Liliane Tenenbaum *

Laboratory of Cellular and Molecular Neurotherapies, Center for Neuroscience Research, Clinical Neurosciences Department, Lausanne University Hospital, Switzerland

ARTICLE INFO

Keywords:
Parvalbumin
Fast-spiking interneurons
Striatum
PV^{Cre} mice
AAV-FLEX vectors

ABSTRACT

PV^{Cre} mice–> combined with AAV-FLEX vectors allowed efficient and specific targeting of PV^{+} interneurons in the striatum. However, diffusion of viral particles to the globus pallidus caused massive transduction of PV^{+} projection neurons and subsequent anterograde transport of the transgene product to the subthalamic nucleus and the substantia nigra pars reticulata.

Different AAV serotypes (1 and 9) and promoters (CBA and human synapsin) were evaluated. The combination of AAV1, a moderate expression level (human synapsin promoter) and a precise adjustment of the stereotaxic coordinates in the anterior and dorsolateral part of the striatum were necessary to avoid transduction of PV^{+} GP projection neurons.

Even in the absence of direct transduction due to diffusion of viral particles, GP PV^{+} projection neurons could be retrogradely transduced via their terminals present in the dorsal striatum. However, in the absence of diffusion, GP-Str PV^{+} projection neurons were poorly or not transduced suggesting that retrograde transduction did not significantly impair the selective targeting of striatal PV^{+} neurons.

Finally, a prominent reduction of the number of striatal PV^{+} interneurons (about 50 %) was evidenced in the presence of the Cre recombinase suggesting that functional effects of AAV-mediated transgene expression in PV^{+} striatal interneurons in PV^{Cre} mice should be analyzed with caution.

1. Introduction

AAV vectors have gained increasing interest for gene therapy of neurological diseases (Kantor et al., 2014; Hocquemiller et al., 2016) as well as for functional studies in neuroscience research (Bedbrook et al., 2018). Targeting specific neuronal subpopulations is a rapidly growing field allowing the manipulation of neuronal circuits using optogenetics (Hunnicutt et al., 2016) or chemogenetics (Woloszynowska-Fraser et al., 2017), the modeling of disease using human disease-causing transgenes (Grames et al., 2018) as well as next-generation targeted gene therapy (Chtarto et al., 2013; Dalkara et al., 2013; Vormstein-Schneider et al., 2020). Thanks to their ability to be axonally transported (Castle et al., 2014), AAV vectors are also useful for anatomical tracing (Zingg et al., 2017).

The cell-type specificity of AAV-mediated transgene expression is dependent on the viral capsid and the regulatory elements driving transcription. Numerous vectors selectively targeting neurons or glial cells have been described. Selective gene expression into neurons can be achieved using pan-neuronal promoters such as the neuron-specific enolase (Klein et al., 1998; Klein et al., 2002) or the synapsin (Kugler et al., 2003; Shevtsova et al., 2005; Dashkoff et al., 2016; Nieuwenhuis, Haenzi et al. 2020) promoters. Specific targeting of excitatory neurons has been described using the calmodulin kinase II (CaMKIIα) promoter (Kim et al., 2015; Watakabe et al., 2015). Oligodendrocytes have been targeted using the myelin-basic protein promoter (Chen et al., 1998, 1999), astrocytes using assembled fragments of the glial fibrillary protein promoter (GFA) (Drinkut et al., 2012; Meunier et al., 2016; Pignataro et al., 2017; Dashkoff et al., 2016) and microglia using the F4/80 or the CD68 promoter (Rosario et al., 2016). In some cases, the cellular specificity is obtained independently of the chosen capsid. For example, the GFA promoter drives expression mainly in astrocytes, when combined with AAV5 (Drinkut et al., 2012), AAV6 (Dirren et al., 2014)

* Corresponding author.
E-mail address: Liliane.Tenenbaum@chuv.ch (L. Tenenbaum).
[1] Both authors equally contributed to this work.
[2] Present address: Division of Neurogeriatrics, Department of Neurobiology, Care Sciences and Society (NVS), Karolinska Institutet, Sweden.

https://doi.org/10.1016/j.jneumeth.2021.109105
Received 12 October 2020; Received in revised form 12 February 2021; Accepted 14 February 2021
Available online 27 February 2021

AAV8 (Pignataro et al., 2017), AAV9 (Dashkoff et al., 2016) or AAV-D/J capsids (Jolle et al., 2019). In contrast, the combination of a cell type-specific promoter and a capsid variant was necessary to transduce microglial cells (Rosario et al., 2016). Finally, brain endothelial cell-specific targeting was obtained using a novel capsid variant combined with a non-specific promoter (chicken β-actin promoter fused to cytomegalovirus enhancer sites) (Korbelin et al., 2016).

The development of vectors selectively targeting neuronal subpopulations is coming of age. Some examples are: GluA4-AAV a capsid variant designed to attach to glutamate receptor 4 (GluA4), selectively expressed by parvalbumin-positive (PV+) interneurons (Geiger et al., 1995), combined with the SFFV (spleen focus-forming virus) promoter (Hartmann et al., 2019); AAV-mDlx a vector targeting interneurons using mDlx transcriptional regulatory elements combined with AAV9 (Dimidschstein et al., 2016) or AAV5 (Lee et al., 2014) capsids; AAV-TH which is targeting dopaminergic neurons thanks to the use of a fragment of the tyrosine hydroxylase promoter (Stauffer et al., 2016) and AAV PHP.eB with hybrid promoters containing specific enhancers targeting PV- and VIP- interneurons (Vormstein-Schneider et al., 2020).

With the advent of single-cell RNA sequencing (Munoz-Manchado et al., 2018; Gokce et al., 2016) and methods for mapping chromatin accessibility (Buenrostro et al., 2015), new synthetic promoters will eventually be identified, which will further refine these molecular tools (Juttner et al., 2019).

Targeting specific neuronal subpopulations can also be achieved using a combination of Cre-driver mice (Hippenmeyer et al., 2005) or rats (Liu et al., 2016) expressing the Cre recombinase under the control of a cell-type specific gene and an AAV vector harboring an inverted ORF flanked by 2 pairs of Cre recognition sites positioned so that expression occurs only when the Cre protein is present (Saunders et al., 2012; Saunders and Sabatini, 2015).

In the striatum, projection neurons, also called medium-sized spiny neurons, relay motor output, expressing D1R- or D2R-type of dopamine receptors which, in response to dopamine respectively activate (D1R) or inhibit (D2R) efferent structures of the motor loop (Surmeier et al., 2007). The striatum also contains several classes of interneurons among which the (PV+) fast spiking and the cholinergic neurons which are thought to coordinate the activity of the projection neurons (Gritton et al., 2019).

In the present study, we have focused on the targeting of PV + interneurons of the dorso-lateral striatum which are key to the control of the sensorimotor striatum (Lee et al., 2017) using PV^{Cre} driver mice (Hippenmeyer et al., 2005).

Limitations of the AAV-FLEX/Cre driver mice targeting system have been previously described: i) off-target expression in cells not expressing Cre (Fischer et al., 2019), ii) expression of Cre in only a part of the targeted neuronal population (Saunders et al., 2016), iii) Cre recombinase-induced cellular abnormalities (He et al., 2014).

We show here that, despite the efficient and specific cellular targeting offered by the Cre-lox system, the AAV delivery parameters have to be precisely adjusted to selectively target the striatum with exclusion of the adjacent globus pallidus containing a high density of PV + projection neurons. Furthermore, PV^{+} striatal interneurons were decreased by the Cre-recombinase. These data suggest that functional effects of AAV-FLEX transgene expression in PV^{+} striatal interneurons in PV^{Cre} mice should be analyzed with caution.

2. Material and methods

2.1. Animals

Pvalbm1(*Cre*)Arbr (PV^{Cre}) mice (www.jax.org: 008069) (Hippenmeyer et al., 2005) in which a IRES-Cre-polyA cassette was introduced in the 3'UTR region of exon 5 of the PV gene, were genotyped using the following primers: Cre-forward, 5' GCG GTC TGG CAG TAA AAA CTA TC 3'; Cre-reverse, 5' GTG AAA CAG CAT TGC TGT CAC TT 3'; PVexon5 forward, 5' CAG AGC AGG CAT GGT GAC TA 3'; PVexon5 reverse, 5' CCA TTC GCC ATT AGT CTG GT 3. PCR conditions were: 4 min at 94 °C followed by 25 cycles of 94 °C for 30 s, 60 °C for 1 min, 72 °C for 1 min.

Eleven weeks-old homozygous PV^{Cre} mice and wild-type (WT) C57Bl6-Ola-Hsd mice (En Vigo) of both sexes were used for all experiments.

2.2. Plasmids

AAV pCAG-FLEX-eGFP-WPRE (Plasmid #51502) and AAV phSyn1 (S)-FLEX-eGFP-WPRE (Plasmid #51504) (Oh et al., 2014) were obtained from AddGene (http://www.addgene.org).

pAAV2/1 and pAAV2/9 were provided by the Penn Vector Core (Philadelphia, Pennsylvania). pAd-helper was purchased from Stratagene (La Jolla, California),

2.3. AAV production

The 3 viruses used in this study were produced by triple transfection of HEK-293 T cells (30 (10 cm) plates; 5.0×10^{6} cells per plate). The AAV helper plasmids; pAAV2/1 or pAAV2/9, expressing the AAV viral genes, were co-transfected with an adeno-helper plasmid (pAd-helper), expressing the adenoviral genes required for AAV replication and encapsidation together with the vector plasmids; AAV-phSyn1- FLEX -eGFP-WPRE or AAV-pCAG-FLEX-eGFP-WPRE in a 2:3:5 M ratio. Fifty hours post-transfection, cells were harvested by low-speed centrifugation, medium was discarded, and cells were resuspended in Tris 50 mM pH 8.5, NaCl 0.1 M, EDTA 1 mM and kept at −20 °C. After five freezing/thawing cycles at −20 °C/37 °C, the cell lysate was centrifuged 20 min at 11,000 rpm. The supernatant was recovered and treated with benzonase (50 units/ml, Sigma) for 30 min at 37 °C and centrifuged again 20 min at 11,000 rpm to eliminate residual debris. The viruses were further purified by iodixanol gradient and microconcentrated as described previously (Zolotukhin et al., 2002). Viral genomes (vg) were titrated by quantitative polymerase chain reaction using universal primers located in the viral ITR sequence as previously described (Aurnhammer et al., 2012). Titers were 1.72×10^{14} vg/ml for AAV1-hsyn- FLEX -eGFP, 1.03×10^{14} vg/ml for AAV9-hsyn- FLEX -eGFP and 5.24×10^{13} vg/ml for AAV9-CBA- FLEX -eGFP.

2.4. Stereotaxic injections

Adult mice (11 weeks-old) were used for unilateral intrastriatal injections. Briefly, the animals were anesthetized with a mixture of ketamine (100 mg/kg, Ketasol, Graeub AG) and xylasine (10 mg/kg, Rompun, Bayer). Injections were made according to coordinates defined by "The Mouse Brain in stereotaxic coordinates, 3rd edition, Franklin, K. B.J. and Paxinos, G. AcademicPress, 2007" using a Kopf stereotaxic apparatus (David Kopf, Tujunga, California). Viral particles diluted in 1 µl of D-PBS (Biowhittaker, Lonza) were infused in the striatum, using a 34 G needle at different coordinates (see Table 1). After injection, the needle was left in place for 5 min in order to allow diffusion of the viral suspension in the parenchyma. The needle was then slowly removed. Animals were maintained in a 12:12 h light-dark cycle with free access to food and water.

Experimental procedures were approved by the "Affaires vétérinaires" of the Canton de Vaud" (Authorization n°VD3400).

2.5. Brain collection and immunohistochemistry

Two weeks after viral injection, mice were euthanized with an overdose of pentobarbital (30 mg/kg in 0.9 % NaCl). A 4 % paraformaldehyde (PFA) solution at pH 7.4 in phosphate buffer saline (PBS, Bichsel AG) was freshly prepared before use. The mice were transcardially perfused consecutively with a PBS solution at pH 7.4 and with the ice-cold 4 % PFA solution. Brains were collected and post-fixed in 4

Table 1
Summary of the coordinates sets and of the number of animals used for each AAV-FLEX virus.

Virus	Coordinates (AP, ML, DV)	Total number of animals	Number of animals with a GP transduction
AAV2/9-CBA-FLEX-eGFP	+1.1, −1.8, −3.0	1	0
	+1.2, −1.8, −3.0	3	2
	+1.0, −1.8, −3.0	3	3
AAV2/9-hsyn-FLEX-eGFP	+1.1, −1.8, −3.0	3	1
	+1.2, −1.8, −3.0	3	2
	+1.2, −1.8, −2.75	3	2
AAV2/1-hsyn-FLEX-eGFP	+1.0, −1.8, −3.0	2	1
	+1.2, −1.8, −2.75	3 + 4*	0

AP: anterio-posterior, ML: mediol-lateral, DV: dorso-ventral, GP: globus pallidus.

* These 4 mice were not included in the analysis of the efficiency and specificity of AAV2/1-hsyn-FLEX-eGFP vector due to a drastic loss of PV-expressing striatal cells in this littermate precluding statistical analysis (see below and Suppl. Fig. 2).

% PFA overnight at 4 °C. Consecutive incubations of 24 h in 20 % and 30 % sucrose solutions were performed to cryoprotect the brains which were then slowly frozen by consecutive immersions in 2-methyl-butane at −10 °C and −20 °C and finally stored at −80 °C. A cryostat (Leica Biosystems, CM1850) was used to collect 25µm-thick coronal sections which were stored in an anti-freeze solution (glycerol 25 %, ethylene glycol 30 % and Na-phosphate buffer 50 mM) at −20 °C. The following antibodies were used to stain PV + cells: guinea pig anti-PV (1:1000, cat. #195004, Synaptic Systems, Göttingen, Germany), biotinylated goat anti-guinea pig (1:200, cat. #BA-7000, Vector Laboratories, Burlingame. USA) and Cy3-conjugated streptavidin (1:300, cat. #016-160-084, Jackson ImmunoResearch Laboratories, West Grove – USA). Free floating sections were stained as follows. Sections were washed 3 times for 10 min in Tris-buffered saline (TBS, 10 mM Tris pH 7.6 and 0.9 % NaCl) at room temperature (RT). Then, they were incubated 1 h at RT in a blocking solution composed of 5 % bovine serum albumin (BSA) in THST buffer (50 mM Tris pH 7.6, 0.5 M NaCl and Triton X-RT100 0.5 %). Afterwards, they were incubated overnight at 4 °C with the primary antibody in a THST solution containing 1 % BSA. The second day, sections were first washed 3 times for 10 min in TBS at RT and then incubated for 1 h at RT with the secondary antibody in THST. Sections were then washed 3 times for 10 min in TBS and incubated in the dark with the streptavidin conjugate for 1 h at RT in THST. Finally, the sections were washed 3 times in PBS for 10 min at RT. The sections were mounted on microscope slides and covered with Vectashield mounting medium (Vector Laboratories, Burlingame, USA).

2.6. Image acquisition and quantifications

Whole slide images were taken with a Zeiss Axioscan Z.1 slide-scanner (Carl Zeiss Microscopy, Germany) using a Plan-Apochromat 10x/0.45 or a Plan-Apochromat 20x/0.8 objective. All the images were taken with an Orca-Flash 4.0 V2 digital CMOS camera. 16 bits images were obtained. Cy3 was excited at 553 nm with a 555/30 nm LED at 50 % power. A beam splitter at 568 nm was used. The detection range was 578−640 nm. eGFP was excited at 493 nm with a 469/38 nm LED at 20 % of power. A beam splitter at 498 was used. Detection range was 507−546 nm. Confocal images were taken with a confocal microscope Zeiss LSM 800 (Carl Zeiss Microscopy, Germany) equipped with a 3x GaAsp detector. All images were collected with a Plan Apochromat 20×/0.8 DIC II objective with a pinhole set at 36 µm. 8 bits resolution images have been obtained by bidirectional scanning and 4x averaging. Cy3 was excited with a 561 nm laser at 0.03 % of power. 739 V of master gain was applied and the detection range was 566−628 nm. eGFP was excited with a 488 nm laser at 0.03 % of power. 750 V of master gain was applied and the detection range was 410−546 nm. Controls with single-fluorescence were performed. No interference between red and green fluorescence was observed.

Images were processed using Zen Blue 2.3 (Carl Zeiss Microscopy, Germany) and ImageJ/Fiji. Z-stacks were acquired on a 25 µm thickness. Shown confocal images in Figs. 1, 2, 5 and 6, are 2D maximal intensity projections of 35 images.

Cells were manually counted on 2D maximal intensity projections of confocal images transformed into the tiff format. Cells were counted by a blind observer using the Multi-point tool in ImageJ. For evaluating the specificity, GFP^+, PV^+, and double-labeled cells were counted. For each animal, five brain sections were selected, and three pictures were taken for each section. To evaluate the efficacy in the dorsal striatum, the striatum was divided in two by a horizontal line, and GFP^+, PV^+, and double-labeled cells were counted in the upper part.

For the quantification of native GFP fluorescence intensity of individual cells (Fig. 6), confocal images were used and the cells were delineated using the "free-hand" selection tool of the ImageJ software. The mean fluorescence intensity was recorded for each individual cell. Area with a similar surface in non-transduced area of the GP or striatum were measured and the obtained values substracted.-

In order to evaluate Cre recombinase effect on PV^+ cells, WT and PV^{Cre} mice were compared. For each AAV-FLEX virus, three WT and three PV^{Cre} successfully injected animals were available. The number of PV^+ cells in the non-injected hemisphere was counted on a section from the same region for each animal and divided by the surface in mm^2. The images were transformed in. jpeg format at a resolution of 300dpi and countings were performed by a blind observer using the Multi-point tool in ImageJ.

To determine viral toxicity the number of PV^+ cells of the injected hemisphere was compared to the corresponding area in the non-injected hemisphere. In order to count cells in the whole striatum, images were acquired with the slide scanner. The images were transformed in. jpeg at a resolution of 300dpi format and cells were counted by a blind observer using the Multi-point tool in ImageJ.

2.7. Statistical analysis

Data analyses and the creation of graphs were performed using GraphPad Prism 8 software (San Diego, CA) for Windows. Comparisons were performed by One-way ANOVA followed by Tukey's multiple comparisons test (Table 2), two-way ANOVA followed by Sidak post hoc test (for more than 2 groups) or by Student *t*-test (2 groups). Results were expressed as mean ± SD and statistical significance was established for a p value ≤ 0.05.

3. Results

3.1. Efficiency and cellular specificity of transgene expression in striatal PV^+ interneurons mediated by AAV2/9-FLEX vectors in PV^{Cre} mice

AAV-FLEX vectors and PV^{Cre} mice were used to target transgene expression into striatal PV^+ interneurons. Since PV expression was weaker in the striatum than in other brain regions (for example in the cerebral cortex; see Suppl. Fig. 1), we used AAV-FLEX vectors (Oh et al., 2014) with strong promoters; the non-specific CMV/chicken β-actin (CBA) promoter (Burger et al., 2004; Klein et al., 2002) or the neuron-specific human synapsin promoter (hsyn) (Shevtsova et al., 2005) combined with the "Woodchuck hepatitis virus post-transcriptional regulatory element" (WPRE) which enhances mRNA stability and protein synthesis (Klein et al., 2002; Oh et al., 2014). In order to further maximize transduction efficiency, the vectors were encapsidated into AAV9 serotype (Cearley and Wolfe, 2006; Klein et al., 2008).

The vectors (7.9×10^9 vg in 1 µl) were injected in the striatum of homozygous PV^{Cre} mice using various coordinates (see Table 1). As a

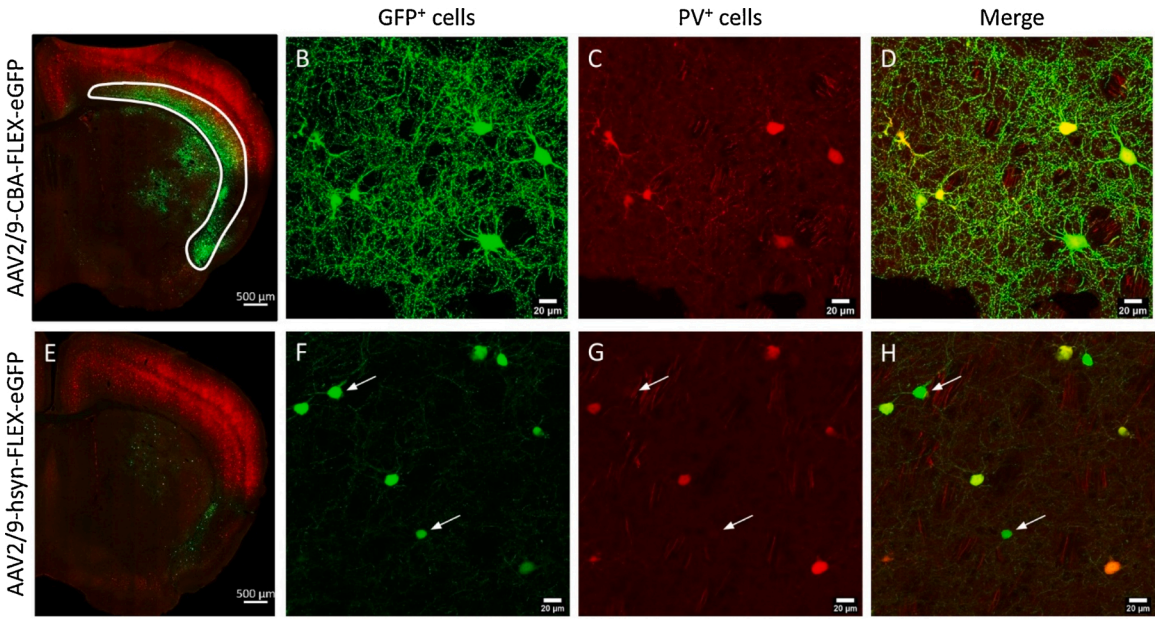

Fig. 1. Efficiency and specificity of AAV2/9-FLEX-mediated PV^{+} striatal interneurons transduction in PV^{Cre} (+/+) mice.
PV^{Cre} (+/+) mice were injected with AAV2/9-CBA-FLEX-eGFP (A, B, C, D) or AAV2/9-hsyn-FLEX-eGFP (E, F, G, H) vectors. A & E, Distribution of GFP^{+} cells in the striatum (Axioscan 20-fold). Confocal pictures showing co-localization (D, H) of native GFP fluorescence (B, F) with parvalbumin staining (C, G). Arrows show cells expressing GFP but without detectable PV staining. Panel A surrounded area: transduced area in the cortex. Control wild-type mice injected with the same vectors did not harbor GFP^{+} cells (data not shown).

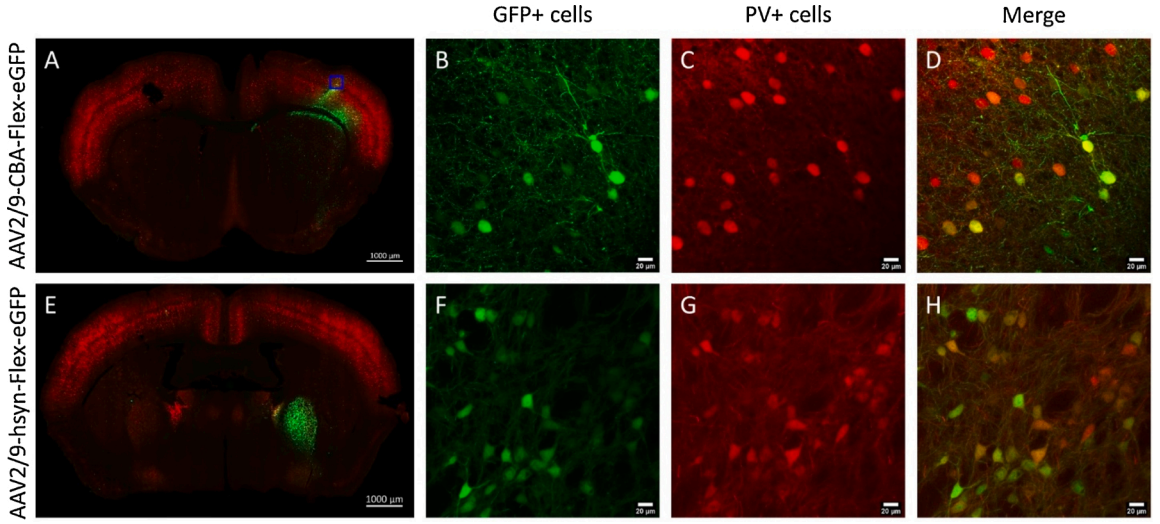

Fig. 2. Efficient transduction of PV^{+} neurons in globus pallidus and cerebral cortex.
PV^{Cre} (+/+) mice were injected with AAV2/9-CBA-FLEX-eGFP (A-D) or AAV2/9-hsyn-FLEX-eGFP (E-H) into the right striatum. GFP^{+} cells were present in the GP (E) and cortex (A). Co-localization (D, H) of native GFP fluorescence (B, F) with parvalbumin staining (C, G). (A, E) have been acquired with a Zeiss Axioscan Z.1 (Carl Zeiss Microscopy, Germany) using a 20x magnification and (B-D & F-H) have been acquired using Zeiss LSM 800 (Carl Zeiss Microscopy, Germany) with a 20× magnification.

negative control, the vectors were also injected in WT C57/Bl6 mice.

GFP^{+} cells were observed in the striatum with a distribution corresponding to the expected pattern of PV^{+} interneurons (Fig. 1A & E). GFP^{+} fibers were more strongly labeled with the CBA promoter (Fig. 1B & D) as compared with the hsyn promoter (Fig. 1F & H), suggesting, that, as expected, the hybrid (cellular/viral) CBA promoter drives a higher transgene expression level than the cellular hsyn promoter.

In order to confirm the cell-type specificity of transgene expression, brain sections were labeled with anti-PV antibodies.

The efficiency of PV^{+} interneurons transduction, evaluated as the number of double-labeled PV^{+}/GFP^{+} cells (Fig. 1D & H), relative to the total number of PV^{+} cells (Fig. 1C & G) was similar (>90 %) for both promoters in AAV2/9 vectors (n = 5 for hsyn and n = 3 for CBA) (Table 2). The specificity of the targeting, evaluated as the number of double-labeled PV^{+}/GFP^{+} cells relative to the total number of GFP^{+} cells (Fig. 1B & F), was approx. 85–90 % for both promoters (Table 2). Few GFP^{+} cells which did not show a detectable PV staining were observed (Fig. 1, arrow), suggesting that a low level of non-specific expression could have occurred. However, injection into WT C57/Bl6 mice did not reveal any GFP^{+} cell (data not shown), suggesting that, as expected GFP expression was dependent on the presence of the Cre recombinase. The GFP^{+} cells which were not labeled by anti-PV antibodies could be due to

Table 2
Percentage of PV/GFP double-labeled cells among total GFP$^+$ cells (specificity) or total PV$^+$ cells (efficiency) in the dorsal striatum.

Virus	Efficiency Double GFPIPV$^+$ among total PV$^+$ (%) (Mean ± SD)	Specificity Double GFPIPV$^+$ among total GFP$^+$ (%) (Mean ± SD)
AAV2/9-CBA-FLEX-eGFP	94.85 ± 3.36	88.69 ± 3.22
AAV2/9-hsyn-FLEX-eGFP	99.49 ± 0.88	84.97 ± 3.56
AAV2/1-hsyn-FLEX-eGFP	93.48 ± 1.72	89.21 ± 2.20

Data were analyzed using one-way ANOVA followed by Tukey's multiple comparisons test. Difference between vectors were not significant for specificity. For efficiency, AAV2/1-hsyn-FLEX-eGFP was significantly lower than AAV2/9-hsyn-FLEX-eGFP ($p = 0.0380$).

a low, undetectable PV expression in these neurons or to a potential toxicity of the Cre recombinase (see below).

3.2. Transduction of contiguous and axonally-connected brain regions

Examination of the whole brains revealed GFP$^+$ cells in the globus pallidus (GP) (Fig. 2E) and in the cerebral cortex (CTX) (Fig. 2A) in a large proportion of the animals. These data suggest that viral particles diffused to these neighboring regions which contain a higher density of PV$^+$ neurons as compared to the striatum (Saunders et al., 2016).

The localized cortical transduction was probably due to a reflux of the viral suspension along the needle and could be avoid using anti-reflux needles (Vazquez et al., 2012; Casanova et al., 2014; Lueshen et al., 2017).

The majority of GFP$^+$ cells also expressed PV in the cerebral cortex (Fig. 2B–D) as well as in the GP (Fig. 2F–H).

Preferential transduction of the GP after injection of AAV vectors in the striatum has been previously reported (Tenenbaum et al., 2000) and was suggested to reflect a preferential diffusion of the viral particles along the vessels driven by the perivascular pump (Hadaczek et al., 2006).

Several stereotaxic coordinates were tested in order to reduce diffusion to extra-striatal areas (see Table 1). The anteroposterior coordinate varied between +1.0 and +1.2, the dorsoventral coordinate varied between -2.75 and -3.0 and mediolateral coordinate was set at -1.8. For both promoters, the majority of the mice harbored a widespread transduction of the GP (see Table 1). With none of the coordinates was the GP transduction avoid in all mice.

3.3. Anterograde transport of GFP from GP PV$^+$ neurons projecting to the SNr and STN

GP contains 40 % of PV$^+$ neurons which project to the subthalamic nucleus (STN), to the substantia nigra pars reticulata (SNr) or to the striatum (Saunders et al., 2016).

Consistently, in animals with GP transduction, GFP$^+$ fibers were evidenced in the STN (Fig. 3A & B) and in the SNr (Fig. 3C & D).

In the striatum, it was not possible to distinguish GFP$^+$ fibers originating from striatal interneurons and pallido-striatal projection neurons. A typical pattern of pallido-striatal fiber tracts was evidenced in WT mice by staining with an anti-PV antibody (Fig. 4A & B). In PV^{Cre} mice in which striatal AAV2/9 injection resulted in transduction of GP PV$^+$ neurons, fiber tracts with the same pattern were GFP$^+$ (Fig. 4C & D), suggesting that, as expected they originate from the pallido-striatal projection neurons.

3.4. Efficiency and cellular specificity of transgene expression in striatal PV$^+$ interneurons mediated by AAV2/1-FLEX vectors in PV^{Cre} mice

Since AAV9 vectors diffusion to the GP and to the CTX hindered the selective targeting of the striatum, we used the AAV1 serotype which has previously been shown to allow region-targeted striatal transduction in

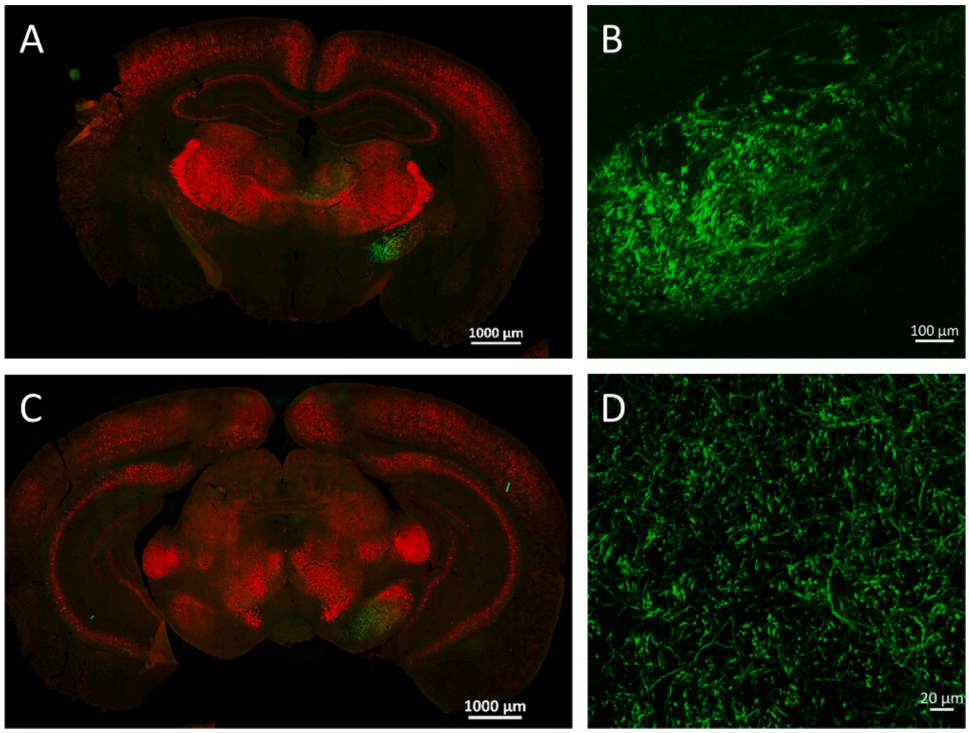

Fig. 3. Anterograde transport of GFP in fibers of GP PV$^+$ neurons projecting to the subthalamic nucleus and to the substantia nigra pars reticulata. PV^{Cre} (+/+) mice were injected with AAV2/9-hsyn-FLEX-eGFP into the right striatum. In mice with a GP transduction, GFP$^+$ fibers were detected in the subthalamic nucleus (STN) (A & B) and in the substantia nigra reticulata (SNr) (C & D). B and D, enlargement of the GFP$^+$ area in the STN (A) and SNr (C), respectively.

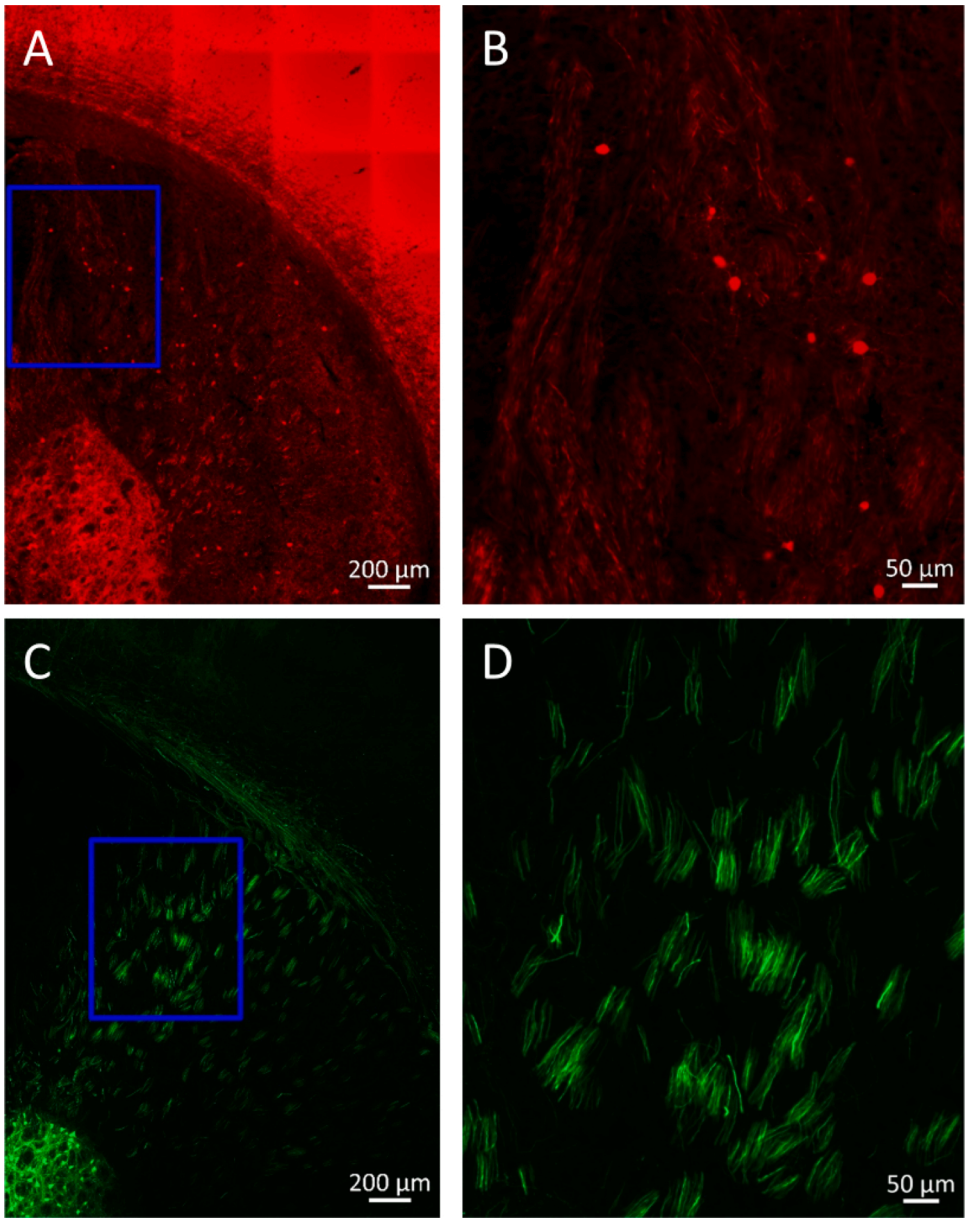

Fig. 4. Anterograde transport of GFP in fibers of GP PV^{+} neurons projecting to the striatum.
(A) PV staining (in red) of a wild-type non-injected mouse. (B) Dorsal striatum PV^{+} interneurons and fibers from pallidal PV^{+} projection neurons. C) Mice with a massive GP transduction show pallido-striatal GFP^{+} fibers in the dorsal striatum (D). (B) Enlargement of the rectangle delineated in (A); (D) enlargement of the rectangle delineated in (C).

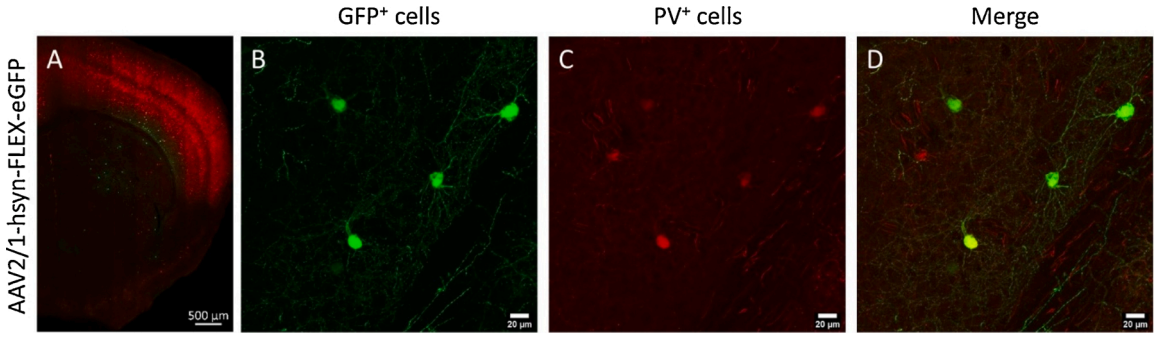

Fig. 5. Efficiency and specificity of AAV2/1-FLEX-hsyn-mediated PV^{+} striatal interneurons transduction in PV^{Cre} (+/+) mice.
PV^{Cre} (+/+) mice were injected with AAV2/1-hsyn-FLEX-eGFP vectors. (A) Distribution of GFP^{+} cells in the striatum (Axioscan 20-fold). Confocal pictures showing co-localization (D) of native GFP fluorescence (B) with parvalbumin staining (C). Control wild-type mice injected with the same vectors did not harbor GFP^{+} cells (data not shown).

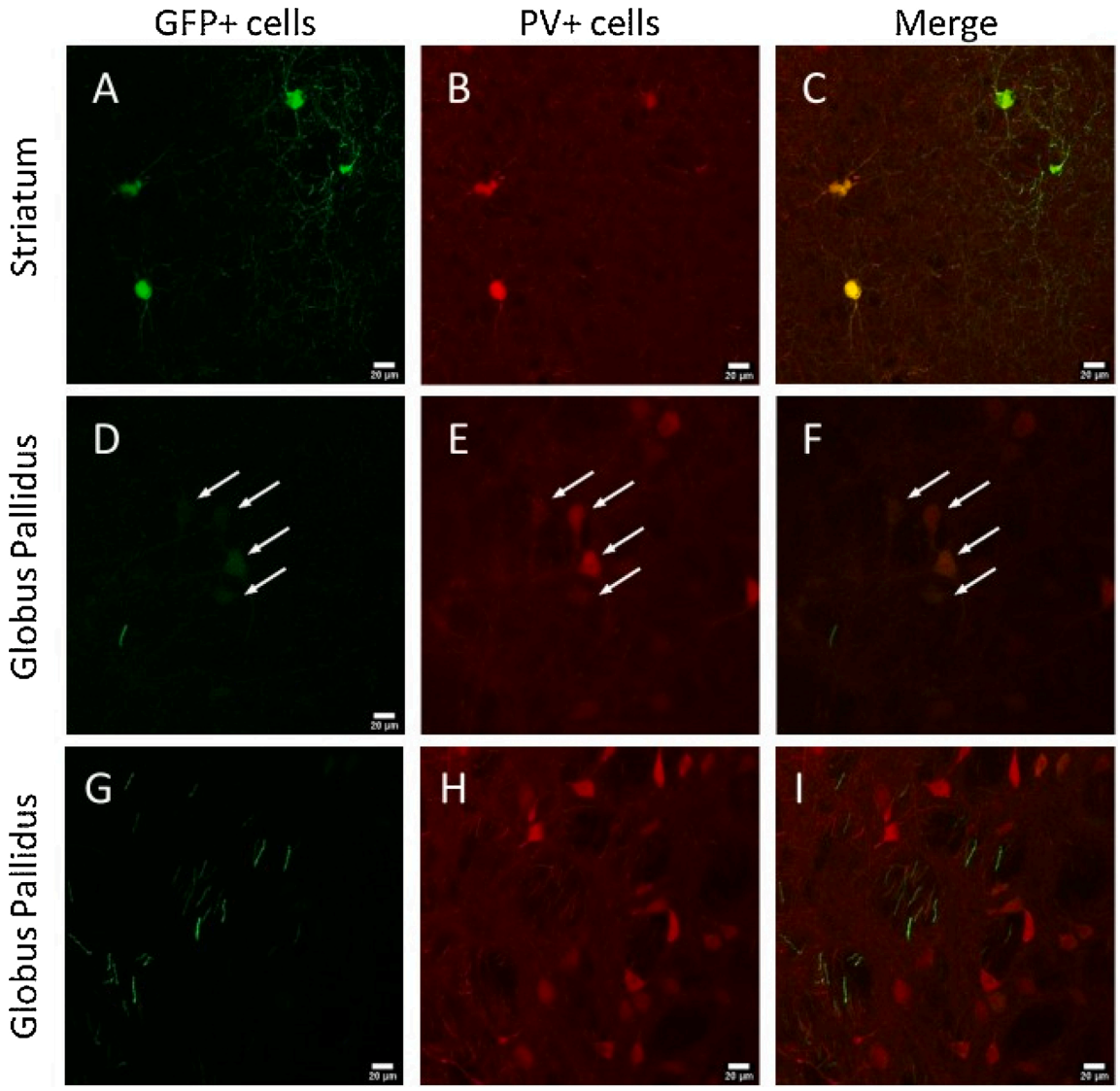

Fig. 6. Retrograde transduction of GP PV^{+} neurons mediated by AAV2/9-hsyn-FLEX-eGFP injected in the dorsal striatum?
PV^{Cre} (+/+) mice were injected with AAV2/9-hsyn-FLEX-eGFP vector. Animals showing no efficient and widespread transduction (as shown in Fig. 2E–H) were further examined.
(A-C) Transduced cells in the dorsal striatum. (D-F) Mice showing 4 GFP^{+} cells in the GP- (G-I) 1 out 2 mice showing GFP^{+} fibers in the GP.

rats (Burger et al., 2004; Bockstael et al., 2008). In mice, however, a moderate number of GFP^{+} cells in the GP were reported after intrastriatal injection of AAV2/1 vectors (Taymans et al., 2007).

Furthermore, since the CBA promoter appeared stronger than the hsyn promoter (Fig. 1), a higher level of GFP expression was obtained in cells distant from the injection site (e.g. note the prominent cortical transduction in Fig. 1A).

Therefore, the hsyn promoter was selected for further experiments. Several stereotaxic coordinates were evaluated to avoid GP transduction. Anteroposterior coordinates varied between +1.0 and +1.2 and dorsoventral coordinates between -2.75 and -3.0. The mediolateral coordinates were set at -1.8. A total of 5 mice were tested. GP transduction could be avoided only with the most anterior and dorsal coordinates (AP=+1.2; ML=−1.8; DV=-2.75) (n = 3) (Fig. 5A).

The efficiency of PV^{+} interneurons transduction, evaluated as the number of double-labeled PV^{+}/GFP^{+} cells (Fig. 5D), relative to the total number of PV^{+} cells (Fig. 5C) was approx. 93 %) (Table 2). The specificity of the targeting, evaluated as the number of double-labeled PV^{+}/GFP^{+} cells relative to the total number of GFP^{+} cells (Fig. 5B), was higher than approx. 89 % (Table 2). As for AAV9, injection into wild-type mice did not result in GFP^{+} cells.

In order to confirm on a larger number of animals that the established stereotaxic coordinates (AP=+1.2; ML=−1.8; DV=-2.75) allow to avoid AAV1 viral particles diffusion to the GP, 4 additional mice, taken from a different littermate of PV^{Cre} (+/+) mice, were injected with AAV2/1-hsyn-FLEX-eGFP. However, in this littermate, the loss of PV^{+} cells in the striatum was aggravated and only few PV^{+} and GFP^{+} cells were observed, precluding a relevant statistical analysis (Suppl. Fig. 2A). However, despite an apparently normal amount of PV^{+} cells in the GP, no GFP^{+} cells were observed (Suppl. Fig. 2B).

3.5. *Retrograde transduction of pallido-striatal neurons by AAV-FLEX vectors?*

Since vectors were injected in the dorsolateral striatum in which pallido-striatal PV^{+} neurons project, in the absence of diffusion, GP PV^{+} neurons could nevertheless be retrogradely transduced.

Therefore, we examined the GP of 4 AAV2/9-hsyn and 3 AAV2/1-hsyn-injected mice apparently devoided of direct GP transduction as shown in Fig. 2E–H.

In one AAV2/9-injected mice, few GFP$^+$ cells were observed in the GP (Fig. 6D). As expected these native GFP fluorescent cells were also PV$^+$ (Fig. 6E & F). However, the level of fluorescence intensity of GFP$^+$ cells in the GP was lower than the fluorescence of directly transduced striatal cells (Fig. 6A), also labeled by anti-PV immunofluorescence (Fig. 6B & C). Whether these GFP$^+$ cells resulted from retrotransduction of pallido-striatal projection neurons or residual diffusion of viral particles remains to be determined. The mean fluorescence intensity of the GFP$^+$ cells in the GP (n = 4) was drastically lower than striatal GFP$^+$ cells in the same animal (n = 4), respectively 5.90 ± 3.69 and 76.98 ± 7.78 A.U.

In 2 other AAV2/9-injected mice, no GFP$^+$ cells were detected in the GP but some fibers were evidenced (Fig. 6G–I). The origin of these GFP$^+$/PV$^+$ fibers in the GP remains to be determined. Finally, in the last AAV2/9-injected mice, no GFP$^+$cells of fibers were observed. These data suggest that if AAV2/9 retrograde transduction of pallido-striatal neurons occurred, it was very inefficient.

In AAV2/1-injected mice, devoided of direct GP transduction, no GFP$^+$ cells were detected in the GP (data not shown).

3.6. Decrease of PV-expressing cells in the striatum of PV^{Cre} mice

Continuous postnatal Cre expression has previously been reported to cause a decrease of cell numbers of some cell types such as immune cells (Schmidt-Supprian and Rajewsky, 2007; Zeitrag et al., 2020) or retinal pigmented epithelium cells (He et al., 2014).

Therefore, we compared the number of PV$^+$ cells in WT and PV^{Cre} homozygous mice.

The number of PV$^+$ cells was drastically (approx. 2-fold) reduced in the striatum (Fig. 7G) but not in the CTX (Fig. 7H) of PV^{Cre} mice as compared to WT mice (compare Fig. 7A–F).

In order to determine whether Cre effect could be aggravated by viral transduction, injected and non-injected hemispheres of PV^{Cre} mice were compared for the 3 vectors (Fig. 7I). No difference was observed. As a control, the number of PV$^+$ cells in the left and right hemispheres of 3 non-injected WT mice were compared. No difference was observed

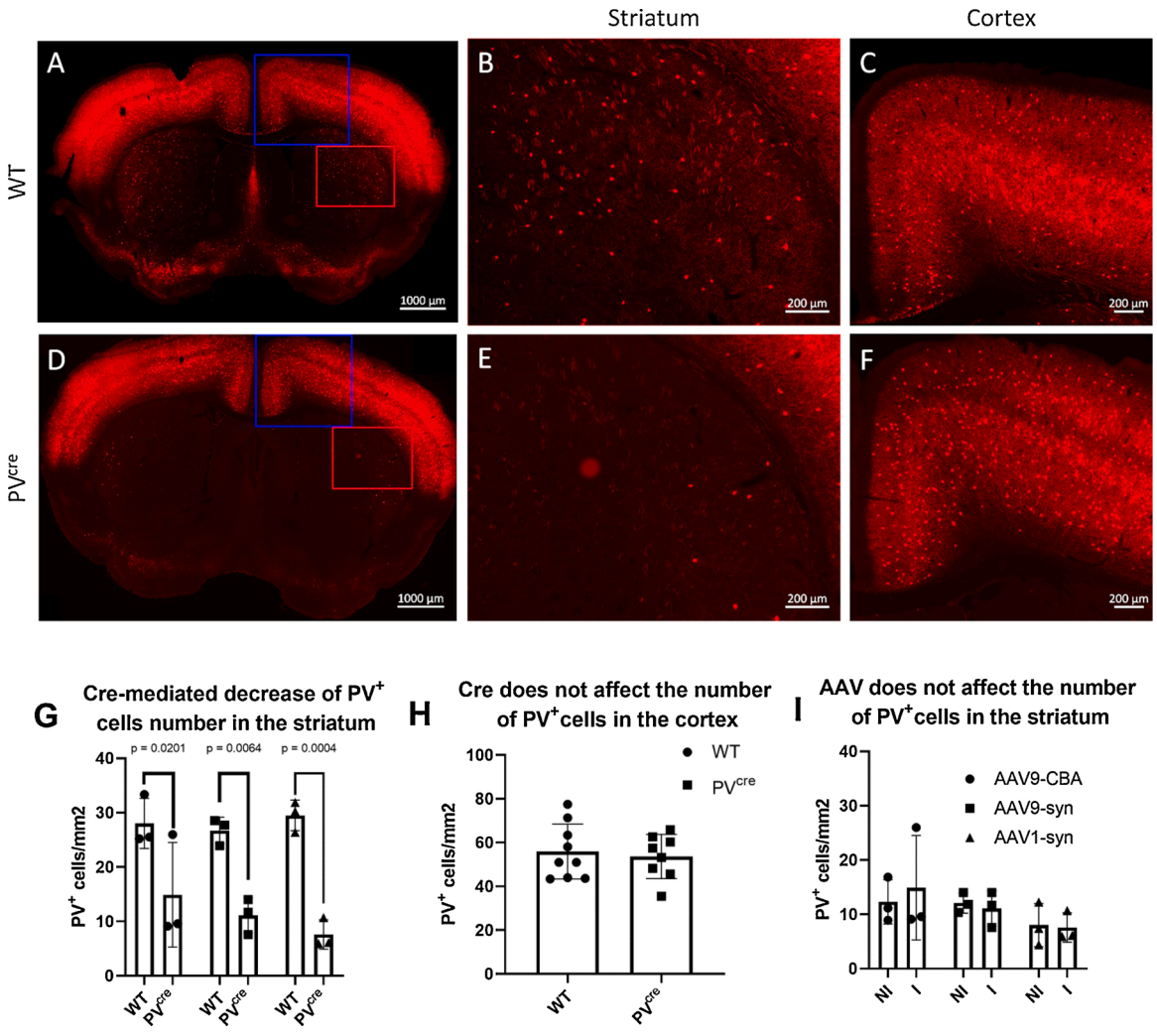

Fig. 7. Decrease of striatal PV$^+$ cells in PV^{Cre} mice.
Wild-type (A-C) and PV^{Cre} (D-F) mice were injected with different AAV-FLEX vectors.
Cre decreases the number of PV$^+$ cells in the striatum but not in the cortex. In the striatum (B & E), the number of PV$^+$ cells was significantly reduced in PV^{Cre} mice (two-way ANOVA with Sidak's multiple comparison test; p = 0.0201 for AAV2/9-CBA-FLEX-eGFP; p = 0.0064 for AAV2/9-hsyn-FLEX-eGFP; p = 0.0004 for AAV2/1-hsyn-FLEX-eGFP) (G). Circles, AAV2/9-CBA-FLEX-eGFP; squares, AAV2/9-hsyn-FLEX-eGFP; triangles, AAV2/1-hsyn-FLEX-eGFP. In the cortex (C & F), the number of PV$^+$ cells in PV^{Cre} mice was not significantly different from the number of PV$^+$ cells in WT mice (Student *t*-test) (H). Circles, wild-type mice; squares, PV^{Cre} mice.
Viral toxicity The number of PV$^+$ cells in the injected hemisphere of PV^{Cre} mice was compared to the contralateral non-injected hemisphere (I). Statistical analysis did not reveal a significant difference (two-way ANOVA with Sidak's multiple comparison test). Circles, AAV2/9-CBA-FLEX-eGFP; squares, AAV2/9-hsyn-FLEX-eGFP; triangles, AAV2/1-hsyn-FLEX-eGFP.

(40.61 ± 3.88 and 39.92 ± 3.19 cells/mm^2 for the right and left hemispheres respectively; student *t*-test: $p = 0.8240$).

4. Discussion

In order to study the role of different types of neurons in complex neuronal circuits, it is crucial to have available molecular tools allowing to selectively deliver genetic information in targeted neuronal subpopulations. Furthermore, it is key to avoid transducing neurons with similar functions in other brain regions which could perturb the behavioral and functional outcomes. Thus, both cell type-specific and region-specific targeting are required.

In the present study, we focused on the targeting of transgene expression into mice PV$^+$ interneurons of the dorsal striatum. These interneurons, also called "fast-spiking", although representing a very small proportion of striatal neurons (approx. 0.5 %), are key to the coordination of striatal projections neurons which modulate the sensory-motor loop.

PV^{Cre} transgenic mice combined with Cre-dependent AAV vectors have been widely used to target PV-expressing neurons in the cerebral cortex, hippocampus and thalamus (Daigle et al., 2018; Madisen et al., 2010). However, very few studies aimed at targeting striatal PV$^+$ interneurons (Abreu et al., 2018; Enterria-Morales et al., 2020).

In order to achieve efficient and selective transduction of striatal PV$^+$ interneurons, we compared 2 different AAV serotypes known to efficiently transduce the CNS, AAV2/1 (Burger et al., 2004; Bockstael et al., 2008) and AAV2/9 (Ciesielska et al., 2013; Klein et al., 2008), and 2 different transcription promoters, the human synapsin (hsyn) and the hybrid chicken β-actin/CMV (CBA) promoters.

We show that, due to the diffusion of viral particles in the brain parenchyma, it is difficult to target the dorsal striatum while avoiding diffusion to the GP. In contrast to the sparse distribution of PV$^+$ striatal interneurons, the GP contains a high density of PV$^+$ neurons (40 % of the total) which project to the STN, the SNr and the striatum (Saunders et al., 2016). Transduction of PV$^+$ GP projection neurons severely compromised the targeting of PV$^+$ striatal interneurons. Precise stereotaxic coordinates adjustment in the dorsolateral striatum, AAV1 capsids (diffusing less than AAV9), and the hsyn promoter (having a moderate transcriptional activity) were necessary to avoid direct transduction of GP PV$^+$ neurons. Such an extrastriatal PV$^+$ neuronal transduction after striatal injections of AAV-FLEX vectors, has been previously described and authors *a posteriori* excluded from their behavioral analysis the animals showing a transduction in untargeted areas (Xu et al., 2016).

None of the vectors provided any GFP$^+$ cell in WT mice demonstrating the tight Cre-dependency of transgene expression. With all tested vectors, the proportion of GFP$^+$ cells stained by anti-PV antibodies was higher than 85 %. However, GFP$^+$ cells not expressing PV at a detectable level were observed. This could be due to an effect of the Cre recombinase towards PV$^+$ neurons. Indeed, we observed that the number of PV$^+$ cells was drastically reduced (~ 2-fold) in the striatum of PV^{Cre} mice. This Cre-mediated effect was specific to striatal PV$^+$ neurons since no reduction of PV$^+$ cells was observed in the cerebral cortex. A similar phenomenon has been reported in retinal pigmented cells in which Cre expression resulted in age- and dosage- dependent attenuation of β catenin and phalloidin stainings in VDM2-Cre mice (He et al., 2014). It remains to be determined whereas Cre effect on PV$^+$ cells is also present in heterozygous Pvalbm1/Arbr mice. During the writing of this manuscript, Enteria-Moralez and collaborators reported a similar effect of Cre towards PV$^+$ cells in the striatum of homozygous Pvalbm1/Arbr mice. In this study, heterozygous Cre (+/-) mice showed a non-significant decrease of PV mRNA. However, the small number of mice ($n = 2$ for some groups) precluded valid statistical analysis.

AAV vectors have previously been reported to have a toxic effect on specific classes of neurons in particular when expressing GFP. Indeed, nigral injection of AAV2/1 vectors in rats resulted in a decrease of the number of TH-expressing neurons, which was further aggravated in the presence of GFP (Albert et al., 2019). AAV2/9 vectors expressing GFP were furthermore shown to elicit an inflammatory response in the rat striatum (Samaranch et al., 2014).

Another potential off-target effect could result from retrograde transport of AAV viral particles in pallidostriatal fibers and transgene expression in GP PV$^+$ projection neurons (Saunders et al., 2016). AAV retrograde transport depends on the capsid serotype and inconsistent data have been reported. For example, AAV1 retrograde transport has been repeatedly found to be negligible (Burger et al., 2004; Bockstael et al., 2008; Oh et al., 2014; Tervo et al., 2016) although another report shows that it occurred with a moderate efficiency in nigrostriatal dopaminergic neurons (Taymans et al., 2007). Surprisingly, efficient retrograde infection was demonstrated with AAV2/1-FLEX vectors in several types of neurons (Rothermel et al., 2013) whereas, in the same study, a constitutive AAV2/1 vector expressing mCherry from the CBA promoter but not one expressing eGFP from the hsyn promoter, was proficient for retrograde transduction. Similarly, inconsistent reports of AAV9 serotype retrograde transport efficiency have been published (Klein et al., 2008; Tervo et al., 2016; Cearley and Wolfe, 2006; Gallagher et al., 2008). In a comparative study, (Tervo et al., 2016) AAV1 ability to undergo retrograde transport was found to be lower than that of AAV9. Different species (rat versus mice), different neuronal pathways, expression levels driven by the chosen promoter and titers of the vector may explain these discrepancies.

To our knowledge, retrograde transduction of GP PV$^+$ neurons following intrastriatal AAV injection has never been described. In our study, in the absence of apparent diffusion, only a very low number of GFP$^+$ cells were detected in 1 out of 4 AAV2/9-injected mice examined, and their native green fluorescence was lower than at the target site in the striatum. Furthermore, it cannot be excluded that the observed GFP$^+$ cells in the GP resulted from a low level of diffusion rather than retrograde transport. In contrast, with AAV2/1 vector, no retrograde transduction of pallidostriatal neurons was observed in our conditions.

In conclusion, caution should be taken when interpreting functional and behavioral data obtained in the PV^{Cre} mice/AAV-FLEX system. First, it is key to avoid transducing PV neurons in other brain regions which will perturb the behavioral and functional outcomes. GP PV$^+$ neurons project to the STN, SNr and striatum (Saunders et al., 2016), nuclei which are all involved in the motor loop. Thus, transduction of these neurons might drastically modify the functional effects of transgene expression. Secondly, the herein described Cre-mediated deleterious effect toward PV$^+$ striatal interneurons could reflect neuronal cell death or loss of PV expression. In the latter case, these neurons are probably dysfunctional since PV, a calcium-binding protein is important for neuronal activity. Perturbation of the synaptic plasticity of these fast-spiking neurons which are thought to coordinate the activity of striatal projection neurons, might severely affect the motor loop. It should be noted that, in a model of AAV-mediated Cre expression, neuronal programmed cell death inducing behavioral perturbations were described (Rezai et al., 2019)

In order to achieve targeted gene delivery into fast-spiking striatal interneurons without the use of PV^{Cre} mice and AAV-Flex vectors, a more selective transcriptional targeting could be designed. Viral vectors with specific enhancers allowing to target neuronal or glial cell populations in wild-type animals are coming to an era (Dimidschstein et al., 2016; Meunier et al., 2016; Pignataro et al., 2017; Vormstein-Schneider et al., 2020).

Authors contribution

Marcelo Duarte-Azevedo: Conceptualization, Methodology, Validation, Formal analysis, Investigation, Data curation, Writing-Review and editing, Visualization.

Sibilla Sander: Conceptualization, Methodology, Validation, Formal analysis, Investigation, Data curation, Writing-Review and

editing, Visualization.

Cheryl Jeanneret: Validation, Formal analysis, Investigation, Data curation, Writing-Review and editing.

Soophie Olfat: Investigation.

Liliane Tenenbaum: Conceptualization, Writing-original draft, Supervision, Project administration, Funding acquisition.

Declaration of Competing Interest

The authors report no declarations of interest.

Acknowledgements

We thank Valentine Golzne for technical assistance.

We thank Jacques Barraud, Geraldine Rochat and Myriam Vuillet (Central animal house, Lausanne University Hospital) for the breeding of PV^{Cre} mice.

Scanning and confocal imaging was performed in CIF Lausanne imaging platform. We thank Luigi Bozzo and Florence Morgenthaler-Grand.

This work was supported by a grant from the Swiss National Foundation (SNF grant number 31003A_179527).

Appendix A. Supplementary data

Supplementary material related to this article can be found, in the online version, at doi:https://doi.org/10.1016/j.jneumeth.2021.109105.

References

Abreu, C.M., Gama, L., Krasemann, S., Chesnut, M., Odwin-Dacosta, S., Hogberg, H.T., Hartung, T., Pamies, D., 2018. Microglia increase inflammatory responses in iPSC-derived human BrainSpheres. Front. Microbiol. 9, 2766.

Albert, K., Voutilainen, M.H., Domanskyi, A., Piepponen, T.P., Ahola, S., Tuominen, R.K., Richie, C., Harvey, B.K., Airavaara, M., 2019. Downregulation of tyrosine hydroxylase phenotype after AAV injection above substantia nigra: caution in experimental models of Parkinson's disease. J. Neurosci. Res. 97 (3), 346–361.

Aurnhammer, C., Haase, M., Muether, N., Hausl, M., Rauschhuber, C., Huber, I., Nitschko, H., Busch, U., Sing, A., Ehrhardt, A., Baiker, A., 2012. Universal real-time PCR for the detection and quantification of adeno-associated virus serotype 2-derived inverted terminal repeat sequences. Hum. Gene Ther. Methods 23 (1), 18–28.

Bedbrook, C.N., Deverman, B.E., Gradinaru, V., 2018. Viral strategies for targeting the central and peripheral nervous systems. Annu. Rev. Neurosci. 41, 323–348.

Bockstael, O., Chtarto, A., Wakkinen, J., Yang, X., Melas, C., Levivier, M., Brotchi, J., Tenenbaum, L., 2008. Differential transgene expression profiles in rat brain, using rAAV2/1 vectors with tetracycline-inducible and cytomegalovirus promoters. Hum. Gene Ther. 19 (11), 1293–1305.

Buenrostro, J.D., Wu, B., Litzenburger, U.M., Ruff, D., Gonzales, M.L., Snyder, M.P., Chang, H.Y., Greenleaf, W.J., 2015. Single-cell chromatin accessibility reveals principles of regulatory variation. Nature 523 (7561), 486–490.

Burger, C., Gorbatyuk, O.S., Velardo, M.J., Peden, C.S., Williams, P., Zolotukhin, S., Reier, P.J., Mandel, R.J., Muzyczka, N., 2004. Recombinant AAV viral vectors pseudotyped with viral capsids from serotypes 1, 2, and 5 display differential efficiency and cell tropism after delivery to different regions of the central nervous system. Mol. Ther. 10 (2), 302–317.

Casanova, F., Carney, P.R., Sarntinoranont, M., 2014. Effect of needle insertion speed on tissue injury, stress, and backflow distribution for convection-enhanced delivery in the rat brain. PLoS One 9 (4), e94919.

Castle, M.J., Gershenson, Z.T., Giles, A.R., Holzbaur, E.L., Wolfe, J.H., 2014. Adeno-associated virus serotypes 1, 8, and 9 share conserved mechanisms for anterograde and retrograde axonal transport. Hum. Gene Ther. 25 (8), 705–720.

Cearley, C.N., Wolfe, J.H., 2006. Transduction characteristics of adeno-associated virus vectors expressing cap serotypes 7, 8, 9, and Rh10 in the mouse brain. Mol. Ther. 13 (3), 528–537.

Chen, H., McCarty, D.M., Bruce, A.T., Suzuki, K., Suzuki, K., 1998. Gene transfer and expression in oligodendrocytes under the control of myelin basic protein transcriptional control region mediated by adeno-associated virus. Gene Ther. 5 (1), 50–58.

Chen, H., McCarty, D.M., Bruce, A.T., Suzuki, K., 1999. Oligodendrocyte-specific gene expression in mouse brain: use of a myelin-forming cell type-specific promoter in an adeno-associated virus. J. Neurosci. Res. 55 (4), 504–513.

Chtarto, A., Bockstael, O., Tshibangu, T., Dewitte, O., Levivier, M., Tenenbaum, L., 2013. A next step in adeno-associated virus-mediated gene therapy for neurological diseases: regulation and targeting. Br. J. Clin. Pharmacol. 76 (2), 217–232.

Ciesielska, A., Hadaczek, P., Mittermeyer, G., Zhou, S., Wright, J.F., Bankiewicz, K.S., Forsayeth, J., 2013. Cerebral infusion of AAV9 vector-encoding non-self proteins can elicit cell-mediated immune responses. Mol. Ther. 21 (1), 158–166.

Daigle, T.L., Madisen, L., Hage, T.A., Valley, M.T., Knoblich, U., Larsen, R.S., Takeno, M. M., Huang, L., Gu, H., Larsen, R., Mills, M., Bosma-Moody, A., Siverts, L.A., Walker, M., Graybuck, L.T., Yao, Z., Fong, O., Nguyen, T.N., Garren, E., Lenz, G.H., Chavarha, M., Pendergraft, J., Harrington, J., Hirokawa, K.E., Harris, J.A., Nicovich, P.R., McGraw, M.J., Ollerenshaw, D.R., Smith, K.A., Baker, C.A., Ting, J.T., Sunkin, S.M., Lecoq, J., Lin, M.Z., Boyden, E.S., Murphy, G.J., da Costa, N.M., Waters, J., Li, L., Tasic, B., Zeng, H., 2018. A suite of transgenic driver and reporter mouse lines with enhanced brain-cell-type targeting and functionality. Cell 174 (2), 465–480 e422.

Dalkara, D., Byrne, L.C., Klimczak, R.R., Visel, M., Yin, L., Merigan, W.H., Flannery, J.G., Schaffer, D.V., 2013. In vivo-directed evolution of a new adeno-associated virus for therapeutic outer retinal gene delivery from the vitreous. Sci. Transl. Med. 5 (189), 189ra176.

Dashkoff, J., Lerner, E.P., Truong, N., Klickstein, J.A., Fan, Z., Mu, D., Maguire, C.A., Hyman, B.T., Hudry, E., 2016. Tailored transgene expression to specific cell types in the central nervous system after peripheral injection with AAV9. Mol. Ther. Methods Clin. Dev. 3, 16081.

Dimidschstein, J., Chen, Q., Tremblay, R., Rogers, S.L., Saldi, G.A., Guo, L., Xu, Q., Liu, R., Lu, C., Chu, J., Grimley, J.S., Krostag, A.R., Kaykas, A., Avery, M.C., Rashid, M.S., Baek, M., Jacob, A.L., Smith, G.B., Wilson, D.E., Kosche, G., Kruglikov, I., Rusielewicz, T., Kotak, V.C., Mowery, T.M., Anderson, S.A., Callaway, E.M., Dasen, J.S., Fitzpatrick, D., Fossati, V., Long, M.A., Noggle, S., Reynolds, J.H., Sanes, D.H., Rudy, B., Feng, G., Fishell, G., 2016. A viral strategy for targeting and manipulating interneurons across vertebrate species. Nat. Neurosci. 19 (12), 1743–1749.

Dirren, E., Towne, C.L., Setola, V., Redmond Jr., D.E., Schneider, B.L., Aebischer, P., 2014. Intracerebroventricular injection of adeno-associated virus 6 and 9 vectors for cell type-specific transgene expression in the spinal cord. Hum. Gene Ther. 25 (2), 109–120.

Drinkut, A., Tereshchenko, Y., Schulz, J.B., Bahr, M., Kugler, S., 2012. Efficient gene therapy for Parkinson's disease using astrocytes as hosts for localized neurotrophic factor delivery. Mol. Ther. 20 (3), 534–543.

Enterria-Morales, D., Lopez-Lopez, I., Lopez-Barneo, J., d'Anglemont de Tassigny, X., 2020. Role of glial cell line-derived neurotrophic factor in the maintenance of adult mesencephalic catecholaminergic neurons. Mov. Disord.

Fischer, K.B., Collins, H.K., Callaway, E.M., 2019. Sources of off-target expression from recombinase-dependent AAV vectors and mitigation with cross-over insensitive ATG-out vectors. Proc. Natl. Acad. Sci. U. S. A. 116 (52), 27001–27010.

Gallagher, P., Watson, S., Elizabeth Dye, C., Young, A.H., Nicol Ferrier, I., 2008. Persistent effects of mifepristone (RU-486) on cortisol levels in bipolar disorder and schizophrenia. J. Psychiatr. Res. 42 (12), 1037–1041.

Geiger, J.R., Melcher, T., Koh, D.S., Sakmann, B., Seeburg, P.H., Jonas, P., Monyer, H., 1995. Relative abundance of subunit mRNAs determines gating and Ca2+ permeability of AMPA receptors in principal neurons and interneurons in rat CNS. Neuron 15 (1), 193–204.

Gokce, O., Stanley, G.M., Treutlein, B., Neff, N.F., Camp, J.G., Malenka, R.C., Rothwell, P.E., Fuccillo, M.V., Sudhof, T.C., Quake, S.R., 2016. Cellular taxonomy of the mouse striatum as revealed by single-cell RNA-Seq. Cell Rep. 16 (4), 1126–1137.

Grames, M.S., Dayton, R.D., Jackson, K.L., Richard, A.D., Lu, X., Klein, R.L., 2018. Cre-dependent AAV vectors for highly targeted expression of disease-related proteins and neurodegeneration in the substantia nigra. FASEB J. 32 (8), 4420–4427.

Gritton, H.J., Howe, W.M., Romano, M.F., DiFeliceantonio, A.G., Kramer, M.A., Saligrama, V., Bucklin, M.E., Zemel, D., Han, X., 2019. Unique contributions of parvalbumin and cholinergic interneurons in organizing striatal networks during movement. Nat. Neurosci. 22 (4), 586–597.

Hadaczek, P., Yamashita, Y., Mirek, H., Tamas, L., Bohn, M.C., Noble, C., Park, J.W., Bankiewicz, K., 2006. The "perivascular pump" driven by arterial pulsation is a powerful mechanism for the distribution of therapeutic molecules within the brain. Mol. Ther. 14 (1), 69–78.

Hartmann, J., Thalheimer, F.B., Hopfner, F., Kerzel, T., Khodosevich, K., Garcia-Gonzalez, D., Monyer, H., Diester, I., Buning, H., Carette, J.E., Fries, P., Buchholz, C. J., 2019. GluA4-targeted AAV vectors deliver genes selectively to interneurons while relying on the AAV receptor for entry. Mol. Ther. Methods Clin. Dev. 14, 252–260.

He, L., Marioutina, M., Dunaief, J.L., Marneros, A.G., 2014. Age- and gene-dosage-dependent cre-induced abnormalities in the retinal pigment epithelium. Am. J. Pathol. 184 (6), 1660–1667.

Hippenmeyer, S., Vrieseling, E., Sigrist, M., Portmann, T., Laengle, C., Ladle, D.R., Arber, S., 2005. A developmental switch in the response of DRG neurons to ETS transcription factor signaling. PLoS Biol. 3 (5), e159.

Hocquemiller, M., Giersch, L., Audrain, M., Parker, S., Cartier, N., 2016. Adeno-associated virus-based gene therapy for CNS diseases. Hum. Gene Ther. 27 (7), 478–496.

Hunnicutt, B.J., Jongbloets, B.C., Birdsong, W.T., Gertz, K.J., Zhong, H., Mao, T., 2016. A comprehensive excitatory input map of the striatum reveals novel functional organization. Elife 5.

Jolle, C., Deglon, N., Pythoud, C., Bouzier-Sore, A.K., Pellerin, L., 2019. Development of efficient AAV2/DJ-based viral vectors to selectively downregulate the expression of neuronal or astrocytic target proteins in the rat central nervous system. Front. Mol. Neurosci. 12, 201.

Juttner, J., Szabo, A., Gross-Scherf, B., Morikawa, R.K., Rompani, S.B., Hantz, P., Szikra, T., Esposti, F., Cowan, C.S., Bharioke, A., Patino-Alvarez, C.P., Keles, O., Kusnyerik, A., Azoulay, T., Hartl, D., Krebs, A.R., Schubeler, D., Hajdu, R.I., Lukats, A., Nemeth, J., Nagy, Z.Z., Wu, K.C., Wu, R.H., Xiang, L., Fang, X.L., Jin, Z.B.,

Goldblum, D., Hasler, P.W., Scholl, H.P.N., Krol, J., Roska, B., 2019. Targeting neuronal and glial cell types with synthetic promoter AAVs in mice, non-human primates and humans. Nat. Neurosci. 22 (8), 1345–1356.
Kantor, B., McCown, T., Leone, P., Gray, S.J., 2014. Clinical applications involving CNS gene transfer. Adv. Genet. 87, 71–124.
Kim, Y., Kim, T., Rhee, J.K., Lee, D., Tanaka-Yamamoto, K., Yamamoto, Y., 2015. Selective transgene expression in cerebellar Purkinje cells and granule cells using adeno-associated viruses together with specific promoters. Brain Res. 1620, 1–16.
Klein, R.L., Meyer, E.M., Peel, A.L., Zolotukhin, S., Meyers, C., Muzyczka, N., King, M.A., 1998. Neuron-specific transduction in the rat septohippocampal or nigrostriatal pathway by recombinant adeno-associated virus vectors. Exp. Neurol. 150 (2), 183–194.
Klein, R.L., Hamby, M.E., Gong, Y., Hirko, A.C., Wang, S., Hughes, J.A., King, M.A., Meyer, E.M., 2002. Dose and promoter effects of adeno-associated viral vector for green fluorescent protein expression in the rat brain. Exp. Neurol. 176 (1), 66–74.
Klein, R.L., Dayton, R.D., Tatom, J.B., Henderson, K.M., Henning, P.P., 2008. AAV8, 9, Rh10, Rh43 vector gene transfer in the rat brain: effects of serotype, promoter and purification method. Mol. Ther. 16 (1), 89–96.
Korbelin, J., Dogbevia, G., Michelfelder, S., Ridder, D.A., Hunger, A., Wenzel, J., Seismann, H., Lampe, M., Bannach, J., Pasparakis, M., Kleinschmidt, J.A., Schwaninger, M., Trepel, M., 2016. A brain microvasculature endothelial cell-specific viral vector with the potential to treat neurovascular and neurological diseases. EMBO Mol. Med. 8 (6), 609–625.
Kugler, S., Lingor, P., Scholl, U., Zolotukhin, S., Bahr, M., 2003. Differential transgene expression in brain cells in vivo and in vitro from AAV-2 vectors with small transcriptional control units. Virology 311 (1), 89–95.
Lee, A.T., Vogt, D., Rubenstein, J.L., Sohal, V.S., 2014. A class of GABAergic neurons in the prefrontal cortex sends long-range projections to the nucleus accumbens and elicits acute avoidance behavior. J. Neurosci. 34 (35), 11519–11525.
Lee, K., Holley, S.M., Shobe, J.L., Chong, N.C., Cepeda, C., Levine, M.S., Masmanidis, S. C., 2017. Parvalbumin interneurons modulate striatal output and enhance performance during associative learning. Neuron 93 (6), 1451–1463 e1454.
Liu, Z., Brown, A., Fisher, D., Wu, Y., Warren, J., Cui, X., 2016. Tissue specific expression of Cre in rat tyrosine hydroxylase and dopamine active transporter-positive neurons. PLoS One 11 (2), e0149379.
Lueshen, E., Tangen, K., Mehta, A.I., Linninger, A., 2017. Backflow-free catheters for efficient and safe convection-enhanced delivery of therapeutics. Med. Eng. Phys. 45, 15–24.
Madisen, L., Zwingman, T.A., Sunkin, S.M., Oh, S.W., Zariwala, H.A., Gu, H., Ng, L.L., Palmiter, R.D., Hawrylycz, M.J., Jones, A.R., Lein, E.S., Zeng, H., 2010. A robust and high-throughput Cre reporting and characterization system for the whole mouse brain. Nat. Neurosci. 13 (1), 133–140.
Meunier, C., Merienne, N., Jolle, C., Deglon, N., Pellerin, L., 2016. Astrocytes are key but indirect contributors to the development of the symptomatology and pathophysiology of Huntington's disease. Glia 64 (11), 1841–1856.
Munoz-Manchado, A.B., Bengtsson Gonzales, C., Zeisel, A., Munguba, H., Bekkouche, B., Skene, N.G., Lonnerberg, P., Ryge, J., Harris, K.D., Linnarsson, S., Hjerling-Leffler, J., 2018. Diversity of interneurons in the dorsal striatum revealed by single-cell RNA sequencing and PatchSeq. Cell Rep 24 (8), 2179–2190 e2177.
Nieuwenhuis, B., Haenzi, B., Hilton, S., Carnicer-Lombarte, A., Hobo, B., Verhaagen, J., Fawcett, J.W., 2020. Optimization of adeno-associated viral vector-mediated transduction of the corticospinal tract: comparison of four promoters. Gene Ther.
Oh, S.W., Harris, J.A., Ng, L., Winslow, B., Cain, N., Mihalas, S., Wang, Q., Lau, C., Kuan, L., Henry, A.M., Mortrud, M.T., Ouellette, B., Nguyen, T.N., Sorensen, S.A., Slaughterbeck, C.R., Wakeman, W., Li, Y., Feng, D., Ho, A., Nicholas, E., Hirokawa, K.E., Bohn, P., Joines, K.M., Peng, H., Hawrylycz, M.J., Phillips, J.W., Hohmann, J.G., Wohnoutka, P., Gerfen, C.R., Koch, C., Bernard, A., Dang, C., Jones, A.R., Zeng, H., 2014. A mesoscale connectome of the mouse brain. Nature 508 (7495), 207–214.
Pignataro, D., Sucunza, D., Vanrell, L., Lopez-Franco, E., Dopeso-Reyes, I.G., Vales, A., Hommel, M., Rico, A.J., Lanciego, J.L., Gonzalez-Aseguinolaza, G., 2017. Adeno-associated viral vectors serotype 8 for cell-specific delivery of therapeutic genes in the central nervous system. Front. Neuroanat. 11, 2.
Rezai Amin, S., Gruszczynski, C., Guiard, B.P., Callebert, J., Launay, J.M., Louis, F., Betancur, C., Vialou, V., Gautron, S., 2019. Viral vector-mediated Cre recombinase expression in substantia nigra induces lesions of the nigrostriatal pathway associated with perturbations of dopamine-related behaviors and hallmarks of programmed cell death. J. Neurochem. 150 (3), 330–340.
Rosario, A.M., Cruz, P.E., Ceballos-Diaz, C., Strickland, M.R., Siemienski, Z., Pardo, M., Schob, K.L., Li, A., Aslanidi, G.V., Srivastava, A., Golde, T.E., Chakrabarty, P., 2016. Microglia-specific targeting by novel capsid-modified AAV6 vectors. Mol. Ther. Methods Clin. Dev. 3, 16026.
Rothermel, M., Brunert, D., Zabawa, C., Diaz-Quesada, M., Wachowiak, M., 2013. Transgene expression in target-defined neuron populations mediated by retrograde infection with adeno-associated viral vectors. J. Neurosci. 33 (38), 15195–15206.
Samaranch, L., San Sebastian, W., Kells, A.P., Salegio, E.A., Heller, G., Bringas, J.R., Pivirotto, P., DeArmond, S., Forsayeth, J., Bankiewicz, K.S., 2014. AAV9-mediated expression of a non-self protein in nonhuman primate central nervous system triggers widespread neuroinflammation driven by antigen-presenting cell transduction. Mol. Ther. 22 (2), 329–337.
Saunders, A., Sabatini, B.L., 2015. Cre activated and inactivated recombinant adeno-associated viral vectors for neuronal anatomical tracing or activity manipulation. Curr. Protoc. Neurosci. 72, 1. 24 21-15.
Saunders, A., Johnson, C.A., Sabatini, B.L., 2012. Novel recombinant adeno-associated viruses for Cre activated and inactivated transgene expression in neurons. Front. Neural Circuits 6, 47.
Saunders, A., Huang, K.W., Sabatini, B.L., 2016. Globus pallidus externus neurons expressing parvalbumin interconnect the subthalamic nucleus and striatal interneurons. PLoS One 11 (2), e0149798.
Schmidt-Supprian, M., Rajewsky, K., 2007. Vagaries of conditional gene targeting. Nat. Immunol. 8 (7), 665–668.
Shevtsova, Z., Malik, J.M., Michel, U., Bahr, M., Kugler, S., 2005. Promoters and serotypes: targeting of adeno-associated virus vectors for gene transfer in the rat central nervous system in vitro and in vivo. Exp. Physiol. 90 (1), 53–59.
Stauffer, W.R., Lak, A., Yang, A., Borel, M., Paulsen, O., Boyden, E.S., Schultz, W., 2016. Dopamine neuron-specific optogenetic stimulation in rhesus macaques. Cell 166 (6), 1564–1571 e1566.
Surmeier, D.J., Ding, J., Day, M., Wang, Z., Shen, W., 2007. D1 and D2 dopamine-receptor modulation of striatal glutamatergic signaling in striatal medium spiny neurons. Trends Neurosci. 30 (5), 228–235.
Taymans, J.M., Vandenberghe, L.H., Haute, C.V., Thiry, I., Deroose, C.M., Mortelmans, L., Wilson, J.M., Debyser, Z., Baekelandt, V., 2007. Comparative analysis of adeno-associated viral vector serotypes 1, 2, 5, 7, and 8 in mouse brain. Hum. Gene Ther. 18 (3), 195–206.
Tenenbaum, L., Jurysta, F., Stathopoulos, A., Puschban, Z., Melas, C., Hermens, W.T., Verhaagen, J., Pichon, B., Velu, T., Levivier, M., 2000. Tropism of AAV-2 vectors for neurons of the globus pallidus. Neuroreport 11 (10), 2277–2283.
Tervo, D.G., Hwang, B.Y., Viswanathan, S., Gaj, T., Lavzin, M., Ritola, K.D., Lindo, S., Michael, S., Kuleshova, E., Ojala, D., Huang, C.C., Gerfen, C.R., Schiller, J., Dudman, J.T., Hantman, A.W., Looger, L.L., Schaffer, D.V., Karpova, A.Y., 2016. A designer AAV variant permits efficient Retrograde access to projection neurons. Neuron 92 (2), 372–382.
Vazquez, L.C., Hagel, E., Willenberg, B.J., Dai, W., Casanova, F., Batich, C.D., Sarntinoranont, M., 2012. Polymer-coated cannulas for the reduction of backflow during intraparenchymal infusions. J. Mater. Sci. Mater. Med. 23 (8), 2037–2046.
Vormstein-Schneider, D., Lin, J.D., Pelkey, K.A., Chittajallu, R., Guo, B., Arias-Garcia, M. A., Allaway, K., Sakopoulos, S., Schneider, G., Stevenson, O., Vergara, J., Sharma, J., Zhang, Q., Franken, T.P., Smith, J., Ibrahim, L.A., astro, Kevin J.M., Sabri, E., Huang, S., Favuzzi, E., Burbridge, T., Xu, Q., Guo, L., Vogel, I., Sanchez, V., Saldi, G. A., Gorissen, B.L., Yuan, X., Zaghloul, K.A., Devinsky, O., Sabatini, B.L., Batista-Brito, R., Reynolds, J., Feng, G., Fu, Z., McBain, C.J., Fishell, G., Dimidschstein, J., 2020. Viral manipulation of functionally distinct interneurons in mice, non-human primates and humans. Nat. Neurosci. 23 (12), 1629–1636.
Watakabe, A., Ohtsuka, M., Kinoshita, M., Takaji, M., Isa, K., Mizukami, H., Ozawa, K., Isa, T., Yamamori, T., 2015. Comparative analyses of adeno-associated viral vector serotypes 1, 2, 5, 8 and 9 in marmoset, mouse and macaque cerebral cortex. Neurosci. Res. 93, 144–157.
Woloszynowska-Fraser, M.U., Wulff, P., Riedel, G., 2017. Parvalbumin-containing GABA cells and schizophrenia: experimental model based on targeted gene delivery through adeno-associated viruses. Behav. Pharmacol. 28 (8), 630–641.
Xu, M., Li, L., Pittenger, C., 2016. Ablation of fast-spiking interneurons in the dorsal striatum, recapitulating abnormalities seen post-mortem in Tourette syndrome, produces anxiety and elevated grooming. Neuroscience 324, 321–329.
Zeitrag, J., Alterauge, D., Dahlstrom, F., Baumjohann, D., 2020. Gene dose matters: considerations for the use of inducible CD4-CreER(T2) mouse lines. Eur. J. Immunol. 50 (4), 603–605.
Zingg, B., Chou, X.L., Zhang, Z.G., Mesik, L., Liang, F., Tao, H.W., Zhang, L.I., 2017. AAV-mediated anterograde transsynaptic tagging: mapping corticocollicular input-defined neural pathways for defense behaviors. Neuron 93 (1), 33–47.
Zolotukhin, S., Potter, M., Zolotukhin, I., Sakai, Y., Loiler, S., Fraites Jr., T.J., Chiodo, V. A., Phillipsberg, T., Muzyczka, N., Hauswirth, W.W., Flotte, T.R., Byrne, B.J., Snyder, R.O., 2002. Production and purification of serotype 1, 2, and 5 recombinant adeno-associated viral vectors. Methods 28 (2), 158–167.